Quantum cascade lasers with an integrated polarization mode converter

D. Dhirhe,[1,*] T. J. Slight,[2] B. M. Holmes,[1] D. C. Hutchings,[1] and C. N. Ironside[1]

[1]*School of Engineering, University of Glasgow, Glasgow, G12 8LT, UK*
[2]*CST Global Ltd, Hamilton International Technology Park, Blantyre, Glasgow, G72 0BN, UK*
[*]*d.dhirhe.1@research.gla.ac.uk*

Abstract: We discuss the design, fabrication and characterization of waveguide polarization mode converters for quantum cascade lasers operating at 4.6 μm. We have fabricated a quantum cascade laser with integrated polarization mode converter that emits light of 69% Transverse Electrical (TE) polarization from one facet and 100% Transverse Magnetic (TM) polarization from the other facet.

OCIS codes: (250.5960) Semiconductor lasers; (310.2790) Guided waves; (310.5448) Polarization, other optical properties.

References and links

1. J. Faist, F. Capasso, D. L. Sivco, C. Sirtori, A. L. Hutchinson, and A. Y. Cho, "Quantum cascade laser," Science **264**(5158), 553–556 (1994).
2. Y. Yao, A. J. Hoffman, and C. F. Gmachl, "Mid-infrared quantum cascade lasers," Nat. Photonics **6**(7), 432–439 (2012).
3. P. Kluczynski, S. Lundqvist, J. Westberg, and O. Axner, "Faraday rotation spectrometer with sub-second response time for detection of nitric oxide using a cw DFB quantum cascade laser at 5.33 μm," Appl. Phys. B: Lasers and Optics **103**(2), 451–459 (2011).
4. A. Roeseler, *Infrared Spectroscopic Ellipsometry* (Akademie-Verlag, 1990).
5. N. Yu, Q. J. Wang, C. Pflugle, L. Diehl, F. Capasso, T. Edamura, S. Furuta, M. Yamanishi, and H. Kan, "Semiconductor lasers with integrated plasmonic polarizers," Appl. Phys. Lett. **94**(15), 151101 (2009).
6. J. J. Bregenzer, S. McMaster, M. Sorel, B. M. Holmes, and D. C. Hutchings, "Compact polarization mode converter monolithically integrated within a semiconductor laser," J. Lightwave Technol. **27**(14), 2732–2736 (2009).
7. J. S. Yu, A. Evans, S. Slivken, and M. Razeghi, "High-performance continuous-wave operation of λ ~ 4.6 μm quantum-cascade lasers above room temperature," IEEE J. Quantum Electron. **44**(8), 747–754 (2008).
8. T. J. Slight, G. Tandoi, D. G. Revin, A. McKee, S. Y. Zhang, W. Meredith, J. W. Cockburn, and C. N. Ironside, "λ ~ 3.35 mm distributed-feedback quantum-cascade lasers with high-aspect-ratio lateral grating," IEEE Photon. Technol. Lett. **23**(7), 420–422 (2011).
9. B. M. Holmes and D. C. Hutchings, "Realization of novel low-loss monolithically integrated passive waveguide mode converters," IEEE Photon. Technol. Lett. **18**(1), 43–45 (2006).
10. D. C. Hutchings and B. M. Holmes, "A waveguide polarization toolset design based on mode beating," IEEE Photon. Journal **3**(3), 450–461 (2011).
11. C. D. Farmer, *Fabrication and evaluation of* $In_{0.52}Al_{0.48}As/In_{0.53}Ga_{0.47}As/InP$ *quantum cascade lasers*, PhD thesis submitted to University of Glasgow, Glasgow (2000).
12. D. Dhirhe, T. J. Slight, C. C. Nshii, and C. N. Ironside, "A tunable single mode double-ring quantum-cascade laser," Semicond. Sci. Technol. **27**(9), 094007 (2012).
13. D. G. Revin, R. S. Hassan, A. B. Krysa, Y. Wang, A. Belyanin, K. Kennedy, C. N. Atkins, and J. W. Cockburn, "Spectroscopic study of transparency current in mid-infrared quantum cascade lasers," Opt. Express **20**(17), 18925–18930 (2012).
14. D. Dhirhe, T. J. Slight, B. M. Holmes, D. C. Hutchings, and C. N. Ironside, "An integrated tunable birefringent filter for quantum cascade lasers," presented at the International Quantum Cascade Lasers School & Workshop 2012, Vienna, Austria, 2–6 Sept. 2012.
15. B. M. Holmes, M. A. Naeem, D. C. Hutchings, J. H. Marsh, and A. E. Kelly, "A semiconductor laser with monolithically integrated dynamic polarization control," Opt. Express **20**(18), 20545–20550 (2012).

1. Introduction

First demonstrated in 1994, Quantum Cascade Lasers (QCLs), based upon semiconductor, intersubband transitions in quantum wells [1], now cover an extensive range of output

#176345 - $15.00 USD Received 18 Sep 2012; revised 15 Oct 2012; accepted 17 Oct 2012; published 29 Oct 2012

wavelengths from the mid-infrared [2] to the far infrared and terahertz. Under the selection rules for intersubband transitions, only interaction with light polarized with the electric field perpendicular to the plane of the quantum wells is allowed. Consequently, in the typical semiconductor optical waveguides employed in quantum cascade lasers, gain is only achieved in Transverse Magnetic (TM) waveguide modes. However, many applications would benefit from an elliptically polarized output, as required in some forms of spectroscopy [3] and ellipsometry [4], and work on producing linearly and right circularly polarized light from QCLs by employing integrated plasmonic polarizers on the output facets of the laser has recently been reported [5].

In this paper we show how it is possible to control the polarization of the light from a QCLs using coupled modes. The work presented here is based upon similar work on conventional interband semiconductor lasers [6] where integrated polarization mode converters (PMCs) are reported. We describe how the design of PMCs are adapted for QCLs and how the PMCs are fabricated and characterized for a QCLs with an emission wavelength of ~4.6 μm.

2. Theory of Polarization Mode Converters (PMCs)

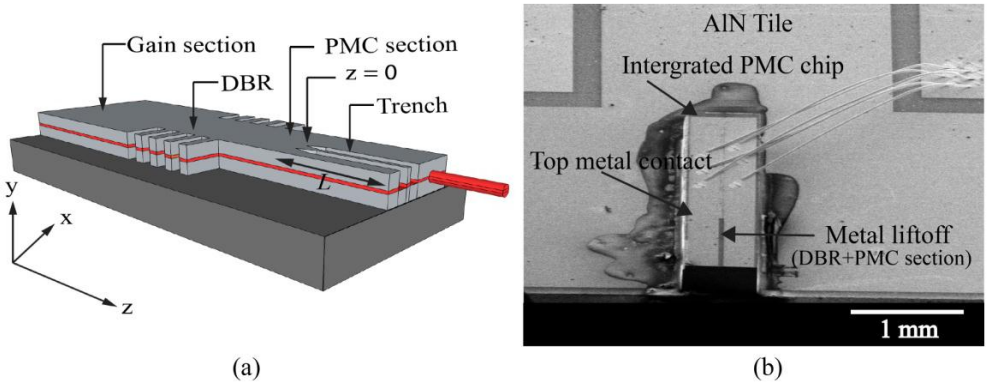

Fig. 1. (a) Schematic illustration of the chip layout of a quantum cascade laser that includes a gain section, lateral distributed Bragg reflector and an integrated polarization mode converter (PMC), the trenches of the PMC were etched using the reactive ion etching lag effect. There is no electrical contact to the PMC section. (b) SEM image of fully fabricated and mounted integrated PMC device.

Figure 1(a) shows a schematic illustration of the integrated PMC and scanning electron micrograph (SEM) image of fully fabricated and mounted integrated PMC device shown in Fig. 1(b). Details of the wafer design can be found in [7] and a discussion of the lateral DFB gratings and be found in [8]. As in the case of conventional interband semiconductor lasers [6], the PMCs are based upon waveguides with asymmetric cross-sectional profiles. This asymmetric cross-section results in a rotation of the optical axis of the birefringent guide, such that as a TM mode enters this asymmetric section, it excites both the single lobed fundamental modes of the guide (Hybrid TE-TM modes), with the relative propagation constant being dependent upon the degree of asymmetry and birefringence of the guide. For an offset of the optical axis of 45 degrees these modes are, essentially, fully hybridised which leads to beating with the characteristics half beat length given by $L = (\pi/\Delta\beta)$, where $\Delta\beta = \beta_1 - \beta_2$ is the difference in propagation constants between two fundamental (single-lobed) modes that propagate in the asymmetric guide [6,9,10]. By varying the length, and/or, the asymmetry of the waveguide, it is possible to adjust the fraction of TM and TE polarization emerging from the asymmetric section, and fabricate waveguide versions of bulk optic polarization components, such as, quarter waveplates or half waveplates. A desirable feature of PMCs, particularly if they are to be incorporated in a QCL resonator, is that they be low loss.

#176345 - $15.00 USD Received 18 Sep 2012; revised 15 Oct 2012; accepted 17 Oct 2012; published 29 Oct 2012

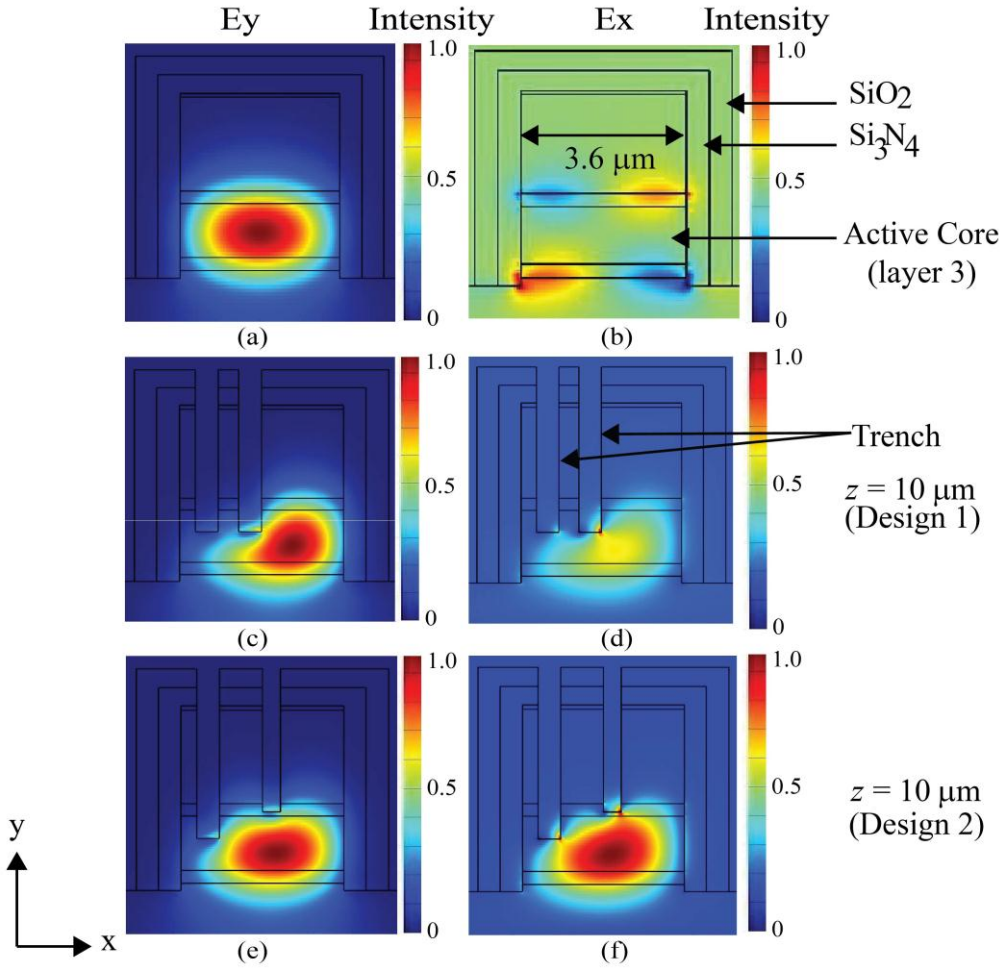

Fig. 2. (a) and (b) Show the simulated mode profiles of the TM and TE components respectively of the lowest order guided mode (without asymmetric cross-section). (c) and (d) show the TM and TE components respectively of the lowest order guided mode within the asymmetric section of design 1. (e) and (f) show the TM and TE components respectively of lowest order guided mode within the asymmetric section of design 2. Both z = 10 μm just after tapered region of PMC.

Design 1 has two trenches of 0.5 μm width on a 3.6 μm wide, and 4.9 μm high waveguide. Design 2 has two trenches, one of 0.5 μm and one of 0.4 μm widths, on a 3.6 μm wide, and 4.9 μm height waveguide. The Table 1 shows the values of refractive indices and thickness of the layers used in the calculation of the mode profile for the TM mode.

To model the operation of the PMC, we first calculate the mode profiles for the hybrid mode in the asymmetric waveguide (Fig. 2) with the hybrid mode separated into TM and TE components at the start of PMC for two different waveguide cross-sections. Figure 2(a)-2(f) shows the mode profile of the TM and TE components of the lowest order guided mode for two designs, optimized using a full-vectorial, 3D eigensolver, as implemented in the software package Lumerical Mode Solutions (LMS). Figure 3(a) shows the normalised TM and TE transmission as a function of propagation distance within the mode conversion sections of two optimised designs. In order to ensure a smooth mode transition with low fluctuation and low insertion losses between the symmetric and asymmetric sections, a graded degree of asymmetry and birefringence (of the guides) were created by tapering the trenches.

#176345 - $15.00 USD Received 18 Sep 2012; revised 15 Oct 2012; accepted 17 Oct 2012; published 29 Oct 2012

Table 1. Refractive indices of the QCL material at λ~4.6 μm as used in the model to calculate TM & TE mode profiles (obtained from [11]).

Layer	Layer name	Semiconductor	Index	Thickness (μm)
6	Contact	InGaAs	3.0	0.1
5	Upper cladding layer	InP	3.008	2.5
4	Upper waveguide	InGaAs/AlInAs	3.39	0.324
3	Active core	InGaAs/AlInAs	3.36	1.447
2	Lower waveguide	InGaAs/AlInAs	3.39	0.344
1	Buffer layer	InP	3.06	0.2
0	Substrate	InP	3.06	-

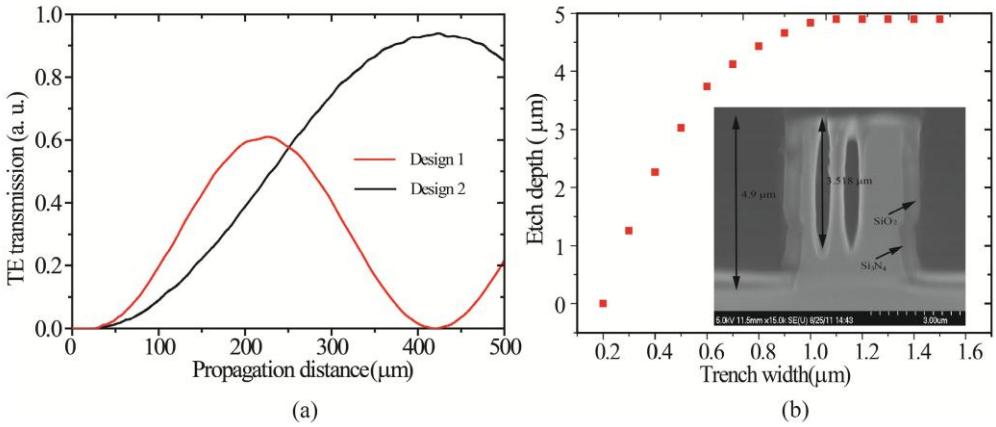

Fig. 3. (a) Calculated TE conversion versus propagation distance using BPM of two designs. (b) Plot of etch depth vs. trench width at etch times of 6 minutes for QCL wafer. Inset SEM image shows the etch profile of a PMC waveguide after ICP etching (design 1).

3. Fabrication of PMCs

The PMC designs used in this work are based upon the fabrication of "trenches" within the waveguide which are positioned to produce an asymmetric cross-sectional profile structure, that results in an effective rotation of the optical axis [9] of the guide. The depth of the trenches was controlled using the reactive ion etching (RIE) lag effect [9,10], where smaller trenches etch at a lower rate than larger ones. The effect was investigated in QCL material using an Inductively Coupled Plasma (ICP) etch tool. The results are given in Fig. 3(b) and clearly show how the etch depth significantly decreases as the trench width drops below 0.8 μm. The advantages of the RIE lag effect for fabricating the PMC include: a one step etch and a naturally occurring taper region of the PMC asymmetric waveguide.

The QCLs used in this work are based upon a double phonon resonant QCL wafer structure reported previously in [7] that emitted at a wavelength of approximately 4.6 μm.

Samples were deposited with 500 nm of SiO_2 to act as a hard mask and coated with ZEP520A positive electron beam resist. Resist patterning was carried out using a Vistec VB6 electron beam lithography (EBL) tool, using a proximity error correction algorithm generated from a Monte Carlo simulation. After the SiO_2 hard mask was formed, using a CF_4/Ar plasma in a standard RIE tool, inductively coupled plasma (ICP) etching in a chlorine/nitrogen (Cl_2/N_2) chemistry was used to define the asymmetric waveguide and DBR grating. 500 nm of Si_3N_4 followed by 500 nm of SiO_2 was deposited as an insulating layer and contact windows were opened on top of the waveguides. Samples were thinned to 200 μm and finally 30 nm Ti, 30 nm Pd and 250 nm Au were deposited to form ohmic top and bottom contacts. Figure 4(a)-4(c) shows the SEM of an integrated PMC device after ICP etching and the inset of Fig. 3(b) shows the cross section of a PMC (design 1). Further information on the fabrication steps can be found in reference [12].

#176345 - $15.00 USD Received 18 Sep 2012; revised 15 Oct 2012; accepted 17 Oct 2012; published 29 Oct 2012

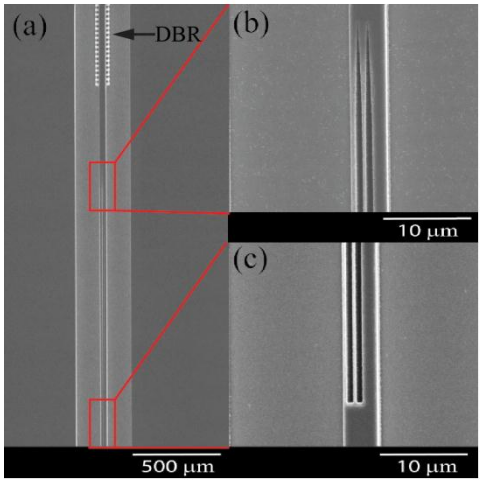

Fig. 4. (a) Shows the SEM top view of integrated PMCs device after ICP etching. (b) Magnified SEM view of taper input section of PMC. (c) Magnified SEM view of output section of PMC.

4. Characterization

The QCLs incorporating PMCs were soldered, epilayer-up, onto aluminum nitride tiles (shown in Fig. 1(b)) and then mounted onto the cold finger of closed cycle helium cryostat. Both the spectral characteristics and optical power were measured using a Bruker Vertex 70 Fourier transform infrared (FTIR) spectrometer. The spectrometer was equipped with a liquid nitrogen cooled indium antimonide (InSb) detector, with a lock-in amplifier used for detector signal recovery. A grid polarizer, comprising 0.12 μm strips of aluminium, on a thallium bromoiodiode (KRS-5) window, was mounted in front of the detector, in a rotatable mount. Design1 characterization was carried out at 298K and design 2 at 250K, with devices driven by 100 ns duration current pulses at a 60 kHz reputation rate.

Figure 5(a) shows the light – injection current (L-I) characteristics of a 265μm long PMC device, based upon design 2, where the power emitted from the PMC facet was measured: a) without the grid polarizer, b) with the grid polarizer axis parallel to QCL waveguide (TM polarization), and c) with the grid polarizer axis perpendicular to the QCL waveguide (TE polarization). The inset in Fig. 5(a) shows the emission spectra measured with similar conditions to those described above. A threshold current density of 2.19 kA/cm^2 was obtained for this device. Polarization purities (= $P_{TE}/(P_{TE} + P_{TM})$ x 100%) of 18% for a 115 μm long PMC (design 1) and 69% for 265μm long (design 2) PMC were obtained from L-I characteristics and emission spectra.

For devices based upon design 1, with 56 μm and 119 μm long PMCs, threshold current densities of 3.25 kA/cm^2 and 3.5 kA/cm^2, respectively, were measured, and for one without a PMC section, 3 kA/cm^2 (Fig. 5(b)).

At a drive current of 1.3$*I_{th}$, an peak optical power of ~2 mW (1.18 mW for TE and 0.53 mW for TM) was measured from the PMC facet for the device with a 265 μm long PMC (design 2) and 18 mW from the gain section facet. However, from measurements of a device with no PMC section, 9 mW was measured at the gain facet, and only 1 mW from the grating facet, implying the majority of the power of our QCLs was emitted from the gain section facets.

For comparison, a 6 μm wide, 3000 μm long, Fabry-Perot (FP) laser processed from the same wafer and measured at 298K, yielded a threshold current density of 2.4 kA/cm^2 with a power of 35 mW at 1.3 $*I_{th}$.

#176345 - $15.00 USD Received 18 Sep 2012; revised 15 Oct 2012; accepted 17 Oct 2012; published 29 Oct 2012

With PMC lengths of around 419 μm (design 2), PMC conversion efficiencies of upto 94% could be obtained. The polarization conversion can approach 100%, but requires increasingly stringent tolerance requirements for a single waveguide element. We have identified an alternative approach of exploiting a universal 50% converter [10] in a half-beat-length which can approach 100% by using two elements.

The polarization of the beam can be determined by recording the detector signal as a function of wire-grid polarizer rotation angle (θ = 0° to 360°), where θ = 0° is defined as the angle of the first maxima in transmission for TM light through the wire grid polarizer. First and for reference, polarization was measured from a DBR QCL laser without PMCs (from front and back facets) and pure TM emission was recorded (red dots) as shown in Fig. 6. For lasers with integrated PMCs, the maxima of the beam intensity was recorded at 20° for design 1 with a 119 μm long PMC and 65° for design 2 with a 265 μm long PMC, as shown in Fig. 6.

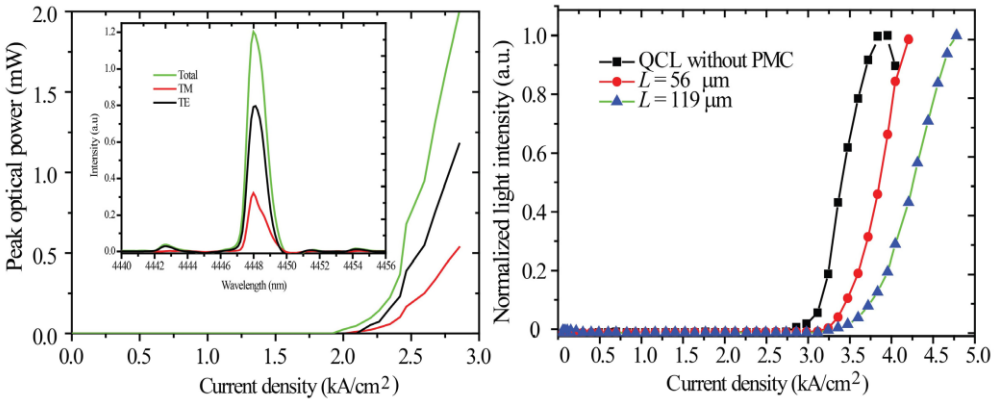

Fig. 5. (a) L-I characteristics of 265μm PMC device with inset showing the TM, TE and total emission spectra. (b) L-I characteristics of QCLs DBR and no PMC, 56 μm PMC and 119 μm PMC.

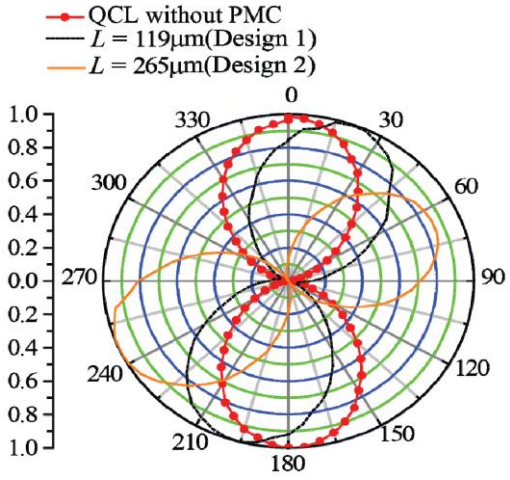

Fig. 6. Polar plots of normalized output power from PMC & DBR facet of the QCL as function of wire-grid polarizer angle for different PMC lengths and asymmetric waveguide cross-sections.

Table 2 shows the relative TE polarization component of different integrated PMCs with PMC lengths experimentally derived from both L-I characteristics and emission spectrum.

#176345 - $15.00 USD Received 18 Sep 2012; revised 15 Oct 2012; accepted 17 Oct 2012; published 29 Oct 2012

The calculated values in Table 2 come from a simulation using the full vectorial 3-D BPM as described above.

Table 2. Compares calculated and measured TE polarization fraction as a function of PMC length.

Design	PMC length (μm)	TE (%) Measured	TE(%) Calculated
1	56	8	7
	71	7	11
	119	18	27
2	256	69	65

To estimate the losses associated with the PMCs, we compared light – threshold current density curves of several QCLs each with different lengths of PMC. The results are summarized in Fig. 5(b) where it can be clearly seen that longer PMCs are associated with higher threshold current densities. From these results it can be estimated that the extra loss introduced by a PMC of design 1 is approximately 6 cm^{-1} estimated from the change in the threshold current density [13] with the length of the PMC. Since the loss for TE light in QCL structures has been reported as lower [13] we attribute the extra loss associated with the PMC to scattering losses arising from the rib and trenches of the PMC and possible modal mismatches at their input and output.

5. Conclusion

We have described the design and fabrication of a PMC for QCLs operating in the mid-infrared and demonstrated that by integrating a PMC with a QCL, the output polarization can be controlled. We have demonstrated that it is possible to have a QCL that emits TM from one facet and predominately (69%) TE from the other facet. We have shown that there is good agreement between our simulation and experiment – for the typical case the simulation predicts to within approximately 10% accuracy. From a consideration of the threshold conditions, with our PMC design (design 1), we have estimated that the increased scattering losses, introduced by the PMCs, are approximately 6 cm^{-1}.

We anticipate that with further optimization, control of the polarization of a QCL will become important in several applications and in the operation of future designs of QCLs. For example, as indicated in [10], if we combine PMCs with an integrated waveguide section that tunes the relative phase between TM and TE modes, a so called differential phase shift (DPS) section, then a tunable integrated birefringent filter [14] can be integrated with a QCL to electronically tune the output wavelength and/or polarization as demonstrated in conventional interband lasers recently [15].

#176345 - $15.00 USD Received 18 Sep 2012; revised 15 Oct 2012; accepted 17 Oct 2012; published 29 Oct 2012